COMPREHENSIVE ANALYSIS OF SINGLE AND COAXIAL SMALL UAS PROPELLERS IN AXIAL FORWARD FLIGHT

Jeffrey D. Sinsay, Science & Technology Corp., Moffett Field, USA
Luke Battey, U.S. Army Combat Capabilities Development Command Aviation & Missile Center, USA
Andrew Milligan, U.S. Army Combat Capabilities Development Command Aviation & Missile Center, USA

Abstract

A comprehensive analysis is used to analyze performance of a small uninhabited aerial system (SUAS) propeller. Various airfoil analysis techniques are explored and verified using single propeller static test data for thrust and power. The SUAS propeller operates in a Reynolds Number range where laminar to turbulent boundary layer transition behavior is historically known to strongly impact airfoil section behavior. Results using various prediction methods for airfoil behavior are compared and discussed with regards to their impact on overall propeller performance prediction accuracy. Predictions of performance and trim are made for a coaxial arrangement of the SUAS propeller, for which future testing is planned.

1. NOTATION

1.1 Symbols

A	Propeller Disk Area, ft^2
C_d	Coefficient of Drag
C_ℓ	Coefficient of Lift
$C_{\ell,\max}$	Maximum Coefficient of Lift
C_P	Coefficient of Power, $P/\rho A V_t^3$
C_T	Coefficient of Thrust, $T/\rho A V_t^2$
M	Mach Number
P	Power, ft-lb/sec
R	Radius, in
r/R	Non-dimensional Radial Position
Re	Reynolds Number
T	Thrust, lb
V	Forward Flight Speed, ft/sec
V_t	Propeller Tip Speed, ΩR, ft/sec
Ω	Propeller Rotational Speed, rad/sec
α	Angle of Attack, deg
η	Propulsive Efficiency, $\mu_z C_T/C_P$
θ_{75}	Collective at 75%R, deg
μ_z	Axial Advance Ratio, V/V_t
ρ	Air Density, slug/ft^3
σ	Propeller Solidity

1.2 Acronyms

AFT	Coder Amplification Factor Transition Model
CA	Comprehensive Analysis
CFD	Computational Fluid Dynamics
ISA	International Standard Atmosphere
LM	Langtry-Menter Transition Model
MB	Medida-Baeder Transition Model
MIT	Massachusetts Institute of Technology
NACA	National Advisory Committee on Aeronautics
NASA	National Aeronautics and Space Administration
RANS	Reynold's Averaged Navier-Stokes
SA	Spalart-Allmaras Turbulence Model
SL	Sea Level
SUAS	Small Uninhabited Aerial System

2. INTRODUCTION

Recently, the U.S. Army Combat Capabilities Development Command Aviation & Missile Center (DEVCOM AvMC) has conducted static thrust and wind tunnel testing on several SUAS propellers in the Army 7- by 10-foot wind tunnel located at NASA Ames Research Center, Moffett Field, CA. This work was follow-on to initial limited testing done in 2019 (Ref. 1), and included the use of a new test stand capable of exploring both pusher/tractor and single/coaxial arrangements. The new stand also allowed for exploration of greater thrust, power and diameters than previously tested. This expanded envelope of performance was desired to support future development of VTOL SUAS vehicles with enhanced range and payload capacity.

Previous work by Kang et. al. (Ref. 2) demonstrated the general applicability of comprehensive analysis (CA) to SUAS performance prediction by making comparisons to the 2019 test data. Airfoil data was generated using the airfoil analysis program XFOIL for a large number of radial stations at a constant Reynolds Number. Correlation between analysis and test was seen to be less accurate at low advance ratio regardless of wake model, indicating potential issues with the 2D sectional data generated from XFOIL.

Work by Cornelius and Schmitz (Ref. 3) compared analytic results with wind tunnel experiment for coaxially mounted propellers. Airfoil data was generated using both XFOIL and the 2D RANS CFD solver ARC2D with fully turbulent boundary layer. The 2D airfoil data was then used with RotCFD, a Hybrid 3D RANS CFD solver, to predict total propeller performance. Better correlation with test data was generally observed for the fully turbulent CFD results, though there was some concern about the potential over-prediction of drag and associated propeller torque. While this approach requires less computational resources than a full 3D RANS CFD solution, it is still appreciably more computationally expensive than the traditional comprehensive analysis approach.

Russell and Sekula (Ref. 4) showed CAMRAD II analysis was capable of capturing trends in performance for SUAS propellers in edgewise flight. For relatively stiff SUAS carbon fiber blades, the effect of elastic vs. rigid blade modeling was shown to have negligible impact on predicted performance. Comparisons between RANS CFD and XFOIL results for airfoil properties showed significant differences in predicted lift and drag. This prediction mismatch was identified as a potential source of the variance in collective pitch required to match forces and power seen in testing.

Challenges in accurately predicting airfoil characteristics for this range of Reynolds Number has previously been identified in Maughmer and Coder (Ref. 5). More recent work (Ref. 6) using models capable of predicting the laminar/turbulent transition point have shown greater accuracy. Work by Kallstrom (Ref. 7) compared application of these approaches to three common full-scale rotorcraft airfoils using the AFTGen airfoil tool. AFTGen provides a common interface for setting up and running sweeps of Mach number and angle of attack necessary for generating airfoil data quickly from multiple airfoil analysis tools, including: XFOIL and OVERFLOW.

The present study further examines the relative trade-off between overall accuracy of solution and computational efficiency by examining propeller performance results using airfoil tables generated from XFOIL and OVERFLOW. Comparison is made with available single propeller static thrust test results to help verify and validate a preferred modeling approach. This same propeller model is then used to study a single propeller in axial flight and a coaxial arrangement of the propellers. Further testing of the single and coaxial arrangement is planned, and will provide an opportunity to assess the accuracy of these pre-test predictions.

3. PROPELLER TESTING OVERVIEW

The Army's new Single and Coaxial Airframe Rotor Test Apparatus (SCARTA) is designed to support testing of propellers in both tractor and pusher configurations, and allow characterization of propeller-body interactional effects. Initial shakedown testing of SCARTA was performed in Fall 2022 in both tractor and pusher configuration. Issues of data quality related to the stand load cell system were identified and corrected, and additional static testing was performed in the Spring 2023 on a modified stand (Figure 1). The static thrust analysis performed as part of this research was validated using this test data.

3.1 Test Stand

Figure 2 shows the overall arrangement of SCARTA when configured for single propeller testing. Details of the coaxial propulsion arrangement are shown in Figure 2b. Individual KDE 10218XF-105 outrunner motors drive each individual propeller. The motors are rated to deliver up to 9.86 hp (7.36 kW) and turn at up to speeds of $>$6,000 rpm. In the coaxial tractor arrangement, the forward motor (motor closest to the propeller hub) is directly mounted to a 6-axis load

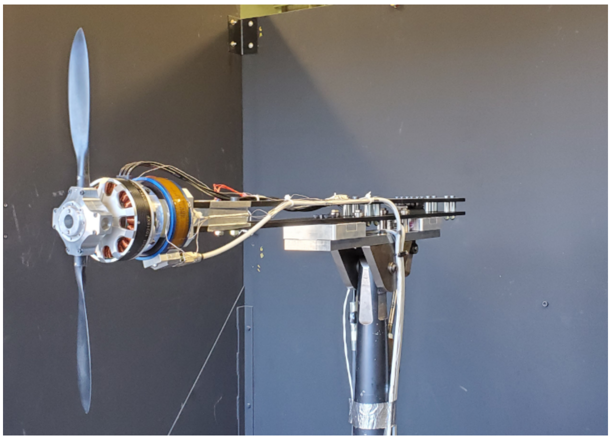

Figure 1: Single propeller static thrust testing on SCARTA, May 2023.

cell and drives the aft propeller. This motor has been modified to allow for a through running shaft from the aft motor which drives the forward propeller. The aft motor mounts to a second 6-axis load cell, which also sees the combined loads of the forward motor and load cell.

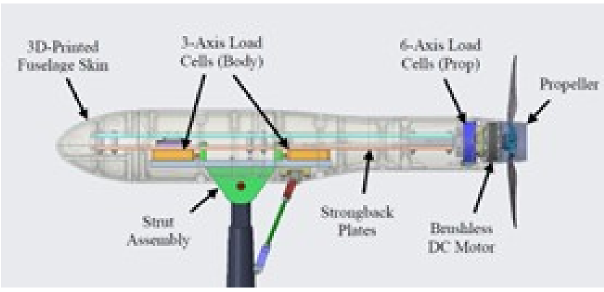

(a) Primary components

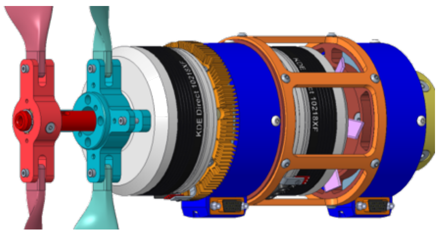

(b) Coaxial motor and propeller arrangement

Figure 2: SCARTA configuration overview

The entire motor and 6-axis load cell assembly is mounted to a metal frame which itself is connected to the support pylon via two 3-axis load cells. The fuselage-like 3D printed center body fairing is also connected to the metal frame. This arrangement of load cells is intended to allow for determination of individual propeller loads and torques as well as fuselage/center body loads. By determining individual propeller loads and fuselage loads with propellers on and off, an estimate of interference effects can be made.

In addition to forces and moments gathered from the load cells, motor voltage, current, rotational speed, and load cell surface temperatures are recorded. These measurements provide two independent measurements of power. The primary one is based on motor torque multiplied by rotational speed and a secondary measure based on motor current and voltage. The validation done in this paper is based on the motor torque based measurement. Temperature measurements are also recorded for the metric and non-metric faces of the 6-axis load cells to support temperature correction of test data. During calibration testing, electric heating mats were added to the load cells to provide preheating. This modification was necessary because during normal operation without preheating, a drift in load cell face temperature was observed as the motors heated up. The resulting temperature gradient of several degrees Celsius across the load cell introduced measurement errors, and it was impossible to find a post-processing temperature correction approach that resulted in accurate and repeatable measurement of zeros and check loads. Preheating the load cells and modulating the heater mats to maintain a constant temperature during testing was found to provide more accurate and repeatable load measurements.

3.2 Propeller

The varioPROP propeller is a commercial, injection-molded, chopped carbon fiber propeller with a rounded root end design that allows for ground adjustment of the collective pitch position of the blades. The particular propeller of interest for the present study, varioPROP 456-16 CFK Propellerblade SG (VP 456-16 SG), was tested on a custom hub mounted to SCARTA. As tested on the custom hub, the propeller diameter is 19.0 in (48.26 cm). The propeller has two blades with a thrust weighted solidity of 0.0644. Both a right-handed and left-handed version of the propeller are available, providing for the ability to test coaxially.

The blade was laser scanned to determine the overall blade geometry. The planform and twist are shown in Figure 3. The propeller has -25° of non-linear twist and a non-linear chord distribution as shown in Figure 3b. The outer 15% of the blade quarter chord is swept aft 8°. The aerodynamic portion of the blade begins at 35%R, with the portion inboard of that radial station comprising a circular cross-section, which interfaces with the hub and allows for manually adjustable pitch variation.

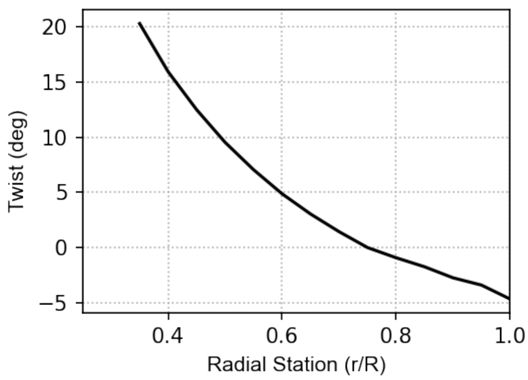

(a) Blade twist

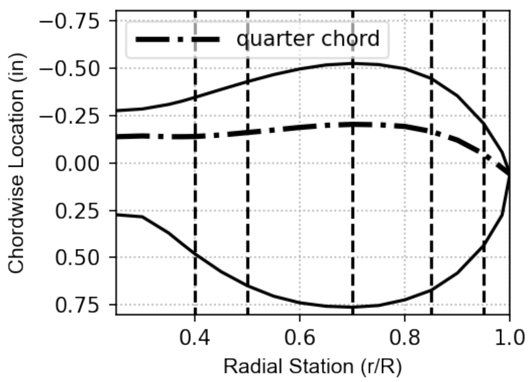

(b) Chord distribution, radial stations for airfoil analysis marked

Figure 3: VP 456-16 SG blade geometry

Figure 4 shows the airfoil cross-sections of the blade, which have a continuous variation in thickness and shape along the radius of the blade. Five cross sections, highlighted in Figure 4 and with spanwise position as identified in Figure 3b, were selected for 2D aerodynamic analysis to generate suitable airfoil force and moment coefficients. The spanwise variation helps to ensure capture of aerodynamic coefficient variation in the blade root to working section transition (40% R and 50%R), primary working section (70%R and 80%R) and tip region (95%R).

4. AIRFOIL SECTION ANALYSIS

Prior to running comprehensive analysis on the VP 456-16 SG propeller, suitable 2D airfoil data for lift, drag and pitching moment were generated. Table 1 lists the associated Mach and Reynolds numbers at

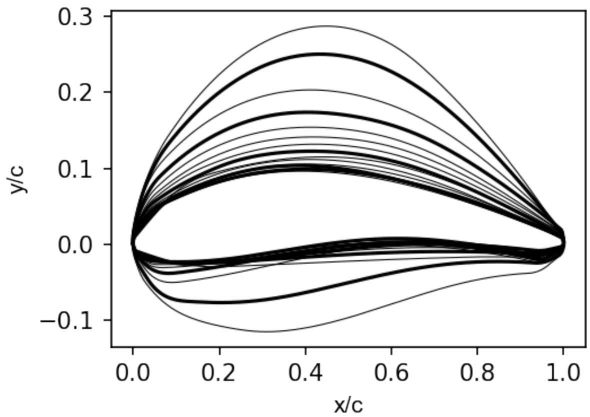

Figure 4: VP 456-16 SG blade airfoil cross-sections, extracted for laser scan, analyzed sections highlighted.

spanwise stations of interest for the propeller operating at a maximum speed of 6,000 rpm at Sea Level Standard Day (SL/ISA). Under these conditions the impact of variation in laminar to turbulent transition in the boundary layer and its associated impact on boundary layer separation behavior is expected to meaningfully contribute to sectional force and moment characteristics. For each airfoil section, a matrix of coefficient values as a function of Mach number (M) and angle of attack (α) is needed. To properly capture the Reynolds number effects, the airfoil data is generated with Reynolds number varying in proportion to Mach number. SL/ISA conditions are used since they closely match the wind tunnel test conditions. For SUAS operating at higher altitudes, separate data tables that correlate Mach and Reynolds number for the prevailing atmospheric conditions may also be required.

For each airfoil section a matrix of runs with Mach number varying from 0.1 to 0.7 and angle of attack from -10° to +24° covered the primary operating range the airfoils may experience. To complete the necessary $\pm 180°$ angle of attack coverage required for C81 (Ref. 8), NACA0012 data was used. To ensure smooth numerical transition from the airfoil analysis data to NACA0012 data, a linear blend between the analysis endpoints at -10° and +24° and the NACA0012 data was used in the range -20° to -10° and +24° to +34° angle of attack. For a propeller in axial flow these extreme angles of attack are not strictly required, but the comprehensive analysis code CAMRAD II requires them for input completeness.

Airfoil force and moment coefficients were calculated for the matrix of Mach and angle of attack using

Table 1: Mach and Reynolds numbers along blade at max operating speed of 6,000 rpm, SL/ISA

Radial Station	Chord (in)	Thickness (% chord)	$\Omega = 6000$ rpm Re $(\times 10^5)$	M	Re $(\times 10^5)$ at M=1
40%R	0.83	31.4	0.91	0.18	5.04
50%R	1.07	18.7	1.46	0.22	6.57
70%R	1.28	13.1	2.45	0.31	7.85
85%R	1.12	11.5	2.58	0.38	6.82
95%R	0.64	12.2	1.66	0.42	3.93
100%R	0.00	n/a	n/a	0.45	n/a

several aerodynamic analysis methods shown previously to provide reasonable results with varying levels of computational cost and accuracy. The lowest computational cost approach was using the airfoil analysis code XFOIL developed at MIT by Mark Drela and Hal Youngren (Ref. 9). XFOIL couples an inviscid vortex panel method with a two-equation integral boundary layer method using an e^N transition model. This approach has been widely used in the design and analysis of low Reynolds number airfoils. Accurate prediction of $C_{\ell,\max}$ is a known deficiency of this code.

A more computationally costly approach was also performed using NASA's CFD code OVERFLOW (Ref. 10). OVERFLOW is a structured grid, Reynolds-averaged Navier-Stokes (RANS) solver with multiple turbulence models. Similar to Kallstrom (Ref. 7), AFTGen was used to generate O-grid airfoil meshes and manage the OVERFLOW executions. The recommended defaults from AFTGen were maintained, except the minimum number of blunt trailing edge points was set to 11, per Kallstrom's findings and the Mach number used for determing the Reynold's number used in the grid y+ calculation was changed from 1.0 to 0.2, consistent with the range of interest for this study.

Computations were performed on the DoD High Performance Computing Modernization Program's Narwhal System. Narwhal provides a standard compute node of 128 2.6 GHz AMD 7H12 Rome cores with 238 GB of memory per node. AFTGen allows for simultaneous execution of alpha, Mach pairings for a single airfoil geometry on one Node of Narwhal using the available 128 cores. Typical wall-clock execution time to generate a C81 table ranged from 1 to 3 hours, with most cases converging within 1 hour.

For this study, the Coder Amplification Factor Transition (AFT) model (Ref. 6) , as implemented in OVERFLOW, is of particular interest. The Coder model uses three equations to predict laminar to turbulent boundary layer transition and provide the additional equations needed for closure to the RANS formulation of the Navier-Stokes equations. The model has been shown to improve correlation of airfoil coefficient prediction with experimental data. This approach in OVERFLOW was compared the fully turbulent Spalart-Allmaras (SA), Medida-Baeder (MB) transition model, and SST with Langtry-Menter (LM) transition. Figures 5 and 6 show these results compared to results from XFOIL for the VP-456-16 SG 70%R airfoil. All methods predict similar values for the lift at zero angle of attack, with XFOIL predicting a slightly steeper lift-curve slope. The value of maximum C_ℓ prediction is similar at low Mach number for XFOIL and fully turbulent SA. However, the shape of the lift curve slope is different between the two predictions; XFOIL at higher angle of attack shows a much sharper initial stall characteristic, which also appears to correspond with a significant shift from mostly laminar to mostly turbulent boundary layer. The SA results have a more gradual loss of lift. The drag prediction for SA is significantly higher than that seen from XFOIL. The minimum drag for all of the OVERFLOW options are in general agreement, suggesting a prediction of little or no laminar boundary layer flow from these models. At higher angle of attack the SA model predicts lower drag compared to the other OVERFLOW models. The three models with boundary layer transition mechanism are very similar in both lift and drag, with the Coder (AFT) and Medida-Baeder (MB) models being virtually indistinguishable. The Langry-Menter (LM) model predicts slightly higher drag and marginally lower $C_\ell, \max$. At Mach 0.7 all of the OVERFLOW models predict significantly more drag and less lift than XFOIL.

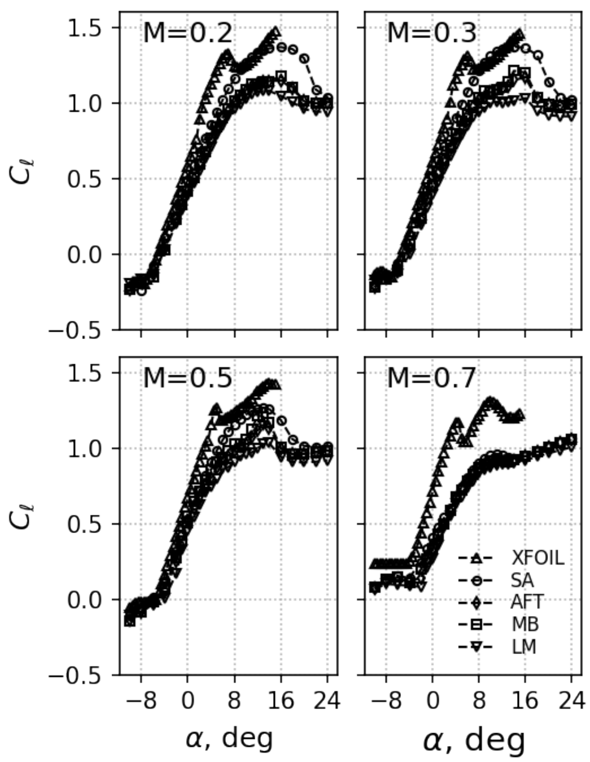

Figure 5: Comparison of predictions for lift versus angle of attack for VP-456-16 SG 70%R airfoil.

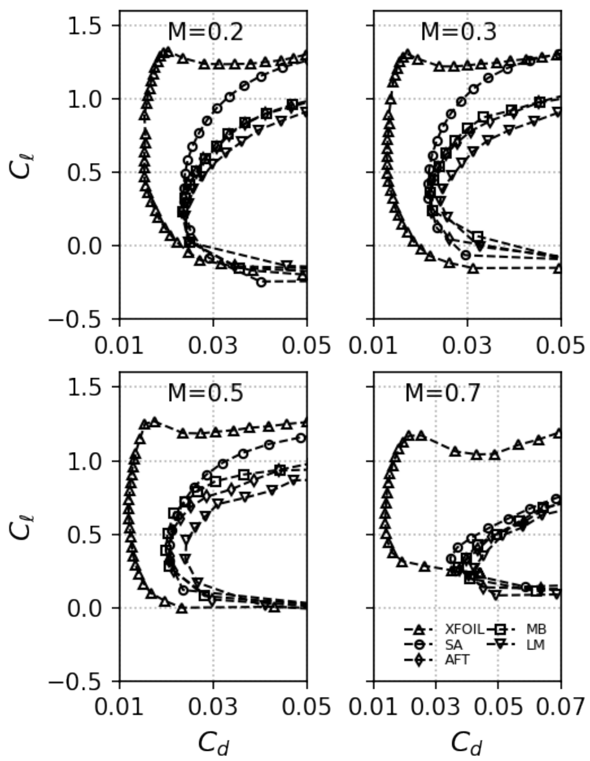

Figure 6: Comparison of predictions for drag versus lift for VP-456-16 SG 70%R airfoil.

Based on the general similarity of the three transition prediction models for the 70%R airfoil, comparisons were made only between XFOIL and OVERFLOW-SA and OVERFLOW-AFT for the remainder of the airfoils. Figures 5–10 show comparisons of lift and drag predictions between these three prediction methods. For the large t/c airfoils, a larger difference in C_ℓ at $\alpha = 0$ is seen that is not present with the more typical airfoil outboard sections. The predicted lift curve slope is similar between all three methods for the 40%R airfoil, however, for the 50%R airfoil, the AFT method predicts a shallower lift curve slope. XFOIL and the SA methods predict generally similar drag for both airfoils, with the AFT predicting significantly higher drag. At higher C_ℓ, the SA predicts a slightly lower drag value than XFOIL.

For the working section and tip airfoils (Figs. 5–6, 9–10), XFOIL and SA predict similar $C_{\ell,\max}$, while AFT predicts a lower value, except at Mach 0.7 where SA and AFT both predict similarly lower values than XFOIL. XFOIL again predicts substantially lower minimum drag and slower increase in drag with lift in the working range, than either OVERFLOW prediction. The AFT approach does predict slightly lower minimum drag compared to SA, but at higher angles of attack SA predicts lower drag.

5. SINGLE PROPELLER ANALYSIS

5.1 Static Thrust

Having generated the necessary 2D airfoil properties, performance predictions for the VP-456-16 SG propeller are made using the comprehensive analysis software CAMRAD II (Ref. 11). The initial focus is on correlation of static thrust from a single propeller with varying RPM and collective pitch settings. The standard hover settings for the free wake model in CAMRAD II are used, with the exception of increasing the extent over which the initial wake convection model is applied to 0.5 revs. This change improves power correlation at higher thrusts, the recommened setting of 0.30 revs (based on 80%R chord) resulted in extremely high non-ideal induced power factors. Due to the high twist of the propeller, static stall delay terms (Ref. 12) are included for both lift and drag. SUAS propellers of this size are generally structurally stiff, and the blades are modeled as a rigid beam with no lead-lag or flapping joints. This form of CA model is typically sufficient for propeller performance analysis. Consistent with the adjustable pitch nature of the VarioProp, a pseudo-pitch bearing and collective control via a swashplate mechanism are included in the

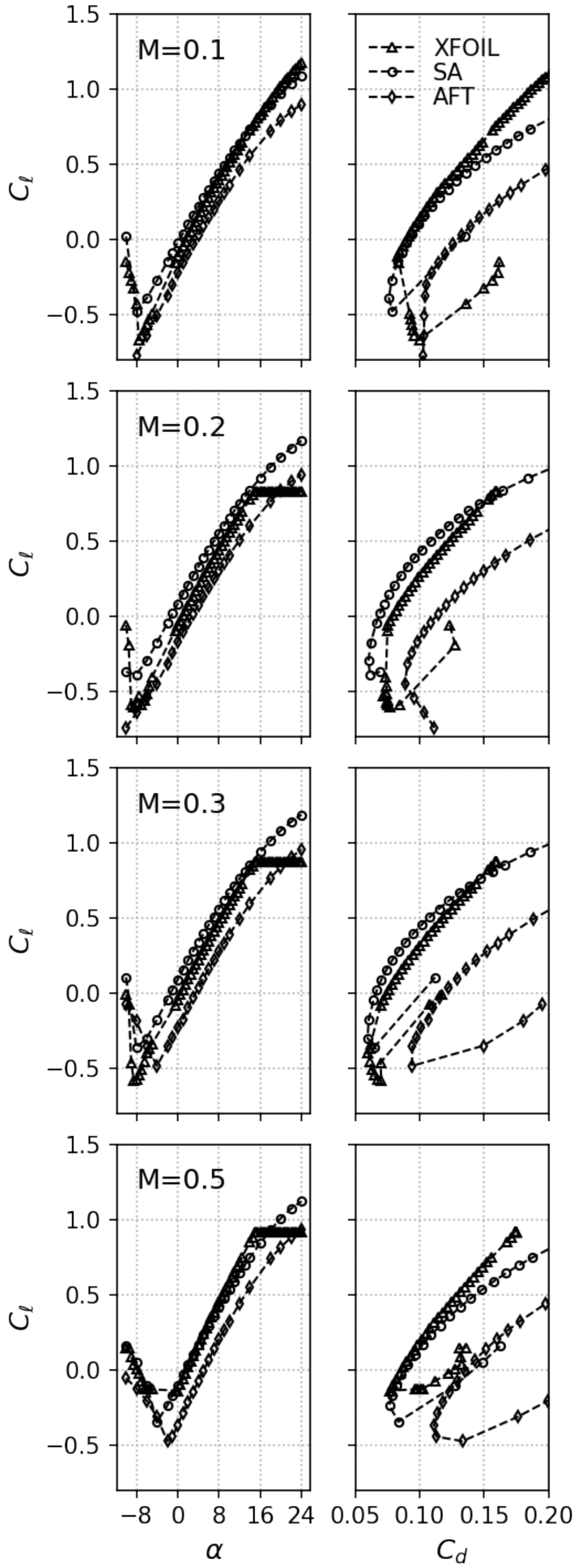

Figure 7: Comparison of calculated lift and drag coefficients for VP-456-16 SG 40%R airfoil at different Mach and Reynolds numbers.

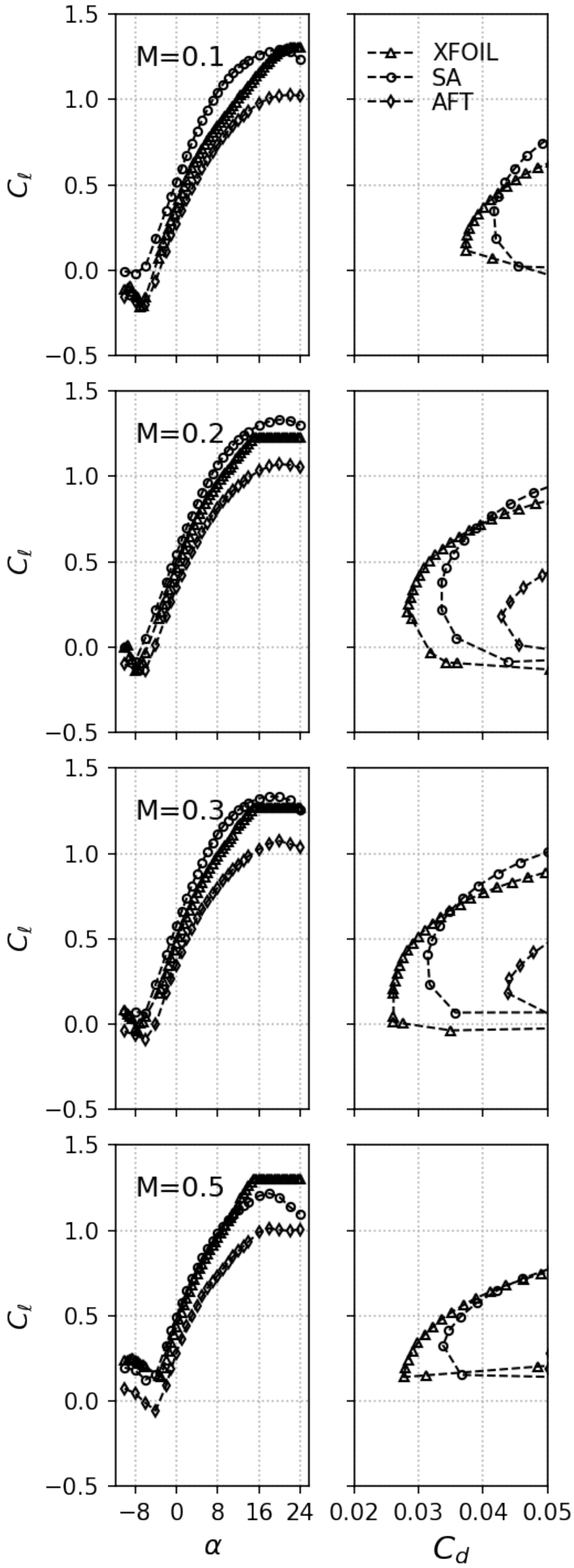

Figure 8: Comparison of calculated lift and drag coefficients for VP-456-16 SG 50%R airfoil at different Mach and Reynolds numbers.

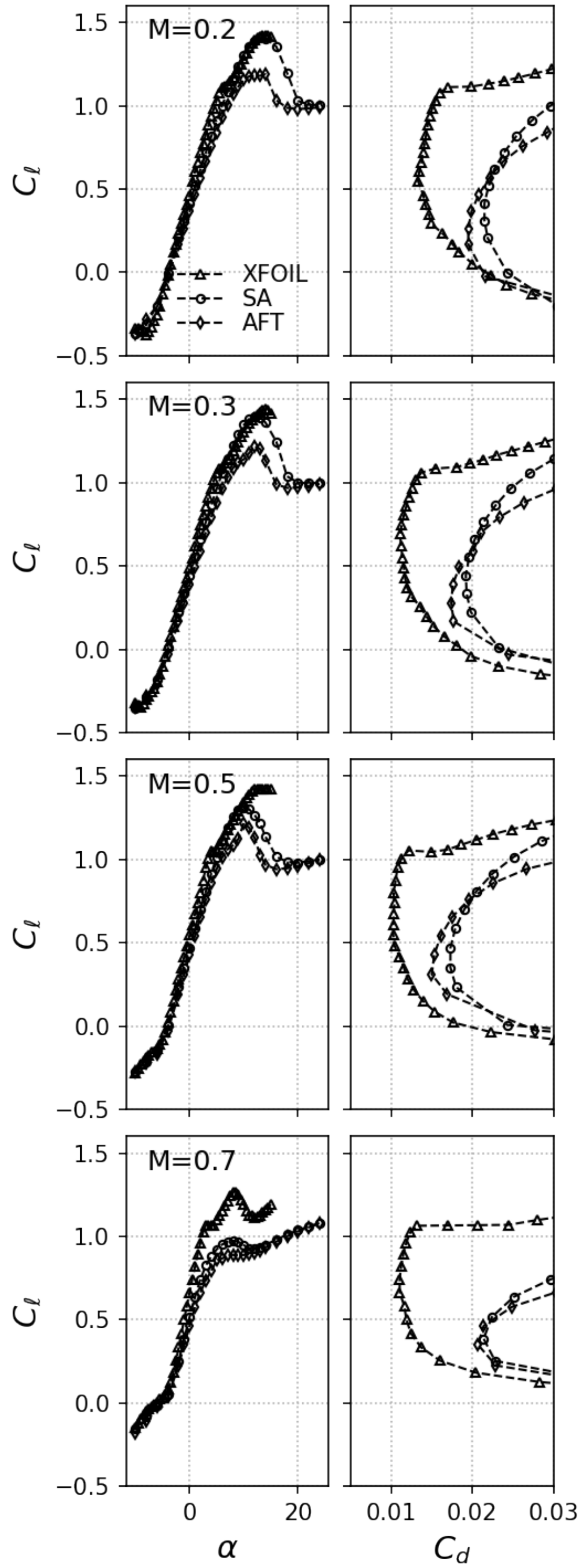

Figure 9: Comparison of calculated lift and drag coefficients for VP-456-16 SG 85%R airfoil at different Mach and Reynolds numbers.

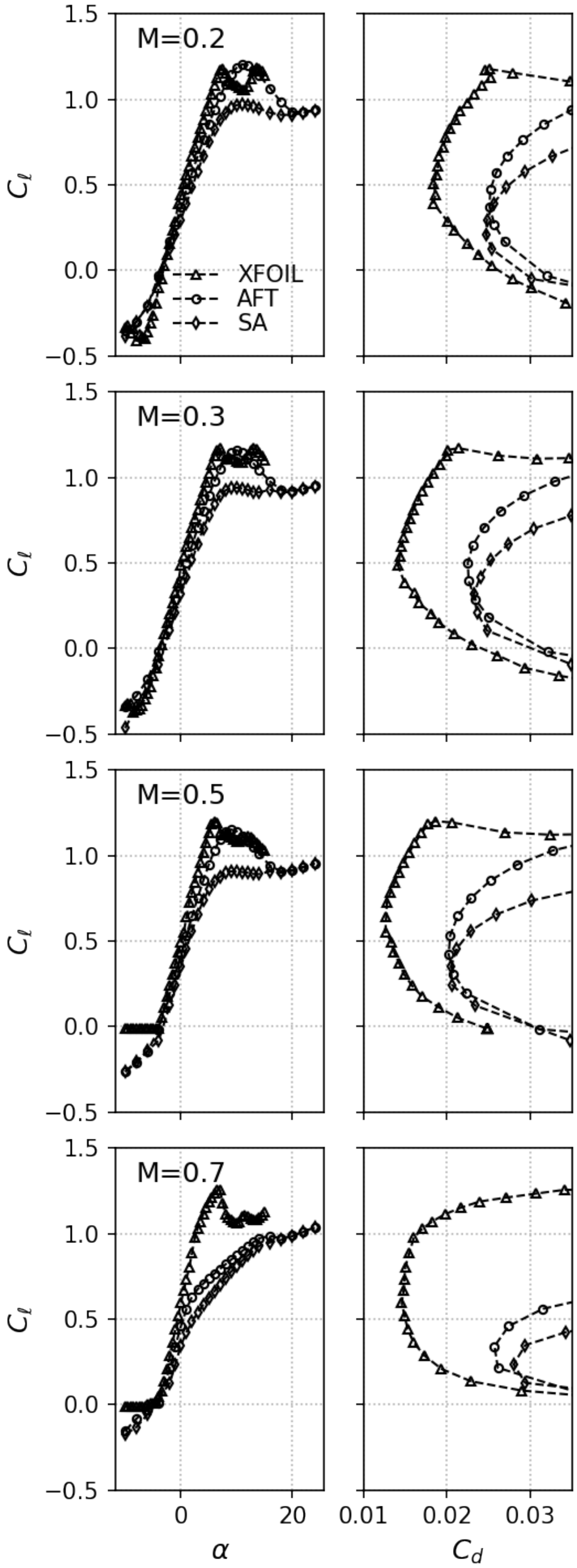

Figure 10: Comparison of calculated lift and drag coefficients for VP-456-16 SG 95%R airfoil at different Mach and Reynolds numbers.

model to simplify analysis when varying blade pitch settings.

The individual C81 airfoil tables are used to define 2D sectional aerodynamic properties along the blade. The blade root cutout extends to r/R=0.25, with the blade divided into five regions: r/R=0.25–0.45, 0.45–0.60, 0.60–0.80, 0.80–0.92, and 0.92–1.00. Each region respectively uses the airfoil coefficients from the 40%R, 50%R, 70%R, 85%R, and 95%R airfoil C81 tables. By assigning each region a unique airfoil coefficient set, potential issues arising from unexpected variation in sectional coefficients due to interpolation along the span are avoided. The lifting line wing in CAMRAD II is divided into 14 aerodynamic segments, which has been shown previously to provide acceptable accuracy, while maintaining computational efficiency.

A comparison of static thrust vs. collective (θ_{75}) is made between the comprehensive analysis (CA) and test data in Figure 11. The CA runs are all identical models and run parameters, except for variation of the propeller airfoil table to be either based on XFOIL, OVERFLOW Spalart-Allmaras (SA), or OVERFLOW Coder Transition (AFT) C81 tables. For the static testing, collective was set using a pitch gauge which was indexed to the blade leading and trailing edges at the r/R=0.75 position. Zero collective is the pitch gauge being parallel the hub plane, where the hub plane itself is defined as perpendicular to the propeller shaft. Figure 11a shows the test data compared to CAMRAD II analysis with collective pitch (r/R=0.75) is set to the same value as the test. As is common for CA, an offset in collective pitch appears to exist between the analysis and reported test data. Figure 11b shows that an assumption of offset in collective of -2.0° for XFOIL and SA runs and -3.0° for AFT runs, brings the test and analysis results into good agreement at the 0° degree collective setting. The slope of thrust vs. collective is similar between the XFOIL and the test results, while the SA and AFT results show a slightly shallower slope. SA results have the best agreement at the highest collective, whereas the XFOIL results have begun flattening, lkely due to airfoil stall. The AFT results are well below the error bars for thrust at higher collectives for both 4,000 and 5,000 rpm even when the collective offset is applied (Fig. 11b).

Figure 12 shows a comparison of predicted torque to test results for 4,000 and 5,000 rpm. The OVERFLOW based CA results match torque well at the low thrust, 0° collective point, but over-predict torque at higher thrusts, with the AFT model significantly over-predicting torque. XFOIL CA results show good agreement in the intermediate thrust levels, within the error bands on torque measurement for the test, but are more conservative at high thrust and under-predict at low thrust. Comparing based on figure of merit in Figure 13, it can be seen that the XFOIL results have generally good agreement on peak figure of merit with the test data, but show a sharper drop in figure of merit, likely due to airfoil stall behavior, at lower C_T/σ than is indicated by the test data. At lower thrust levels, the XFOIL results over-predict figure of merit. OVERFLOW-AFT results significantly under-predict both peak figure of merit and C_T/σ where figure of merit begins to decrease because of stall. OVERFLOW-SA results are closer to test data, but still generally under-predict peak figure of merit and C_T/σ where it is obtained. The OVERFLOW results, however, are more accurate at matching test figure of merit results at the low thrust point.

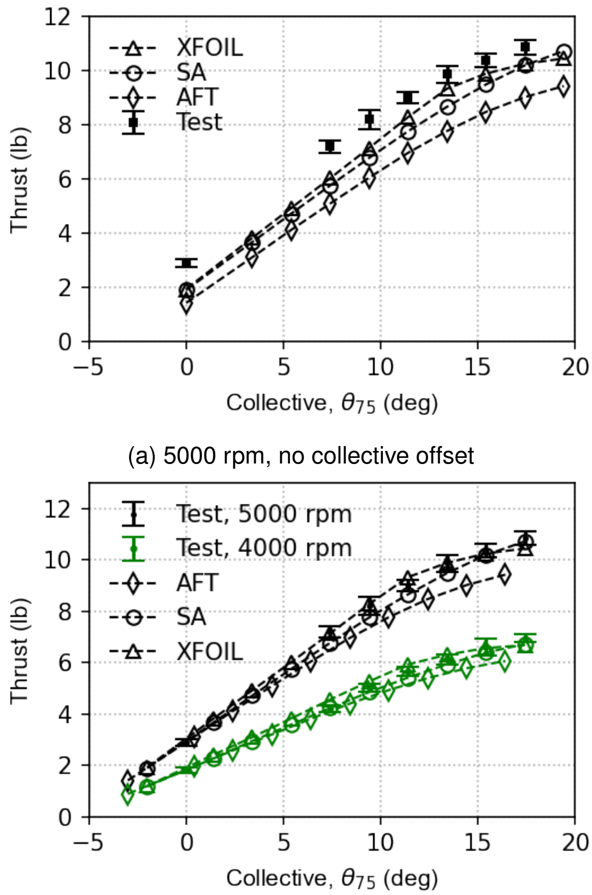

(a) 5000 rpm, no collective offset

(b) Collective offset: XFOIL/SA=-2° AFT=-3°

Figure 11: Comparison of test and analysis thrust vs. collective for two RPMs.

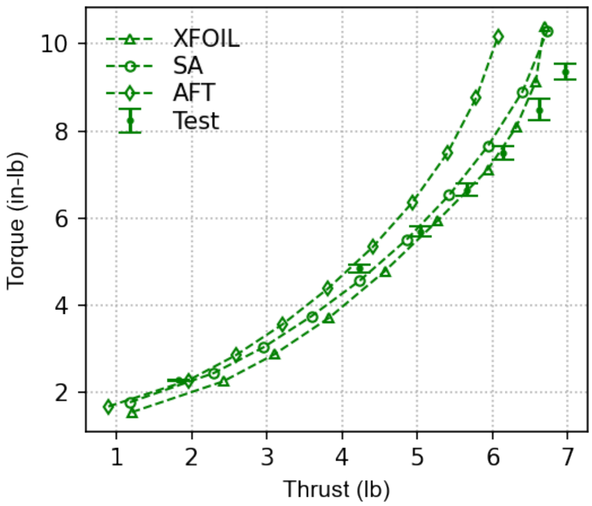

(a) 4000 rpm

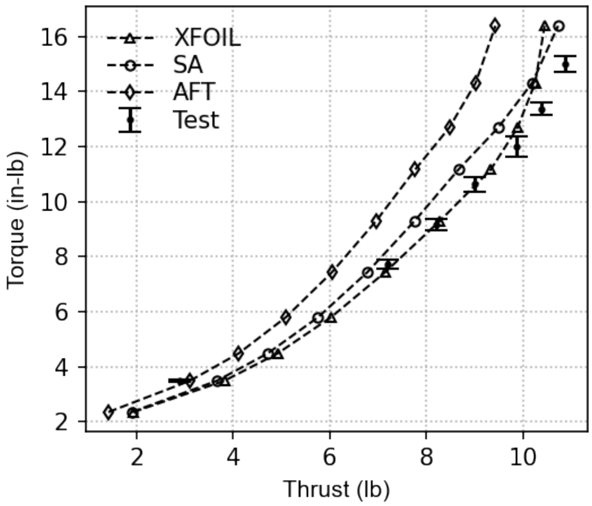

(b) 5000 rpm

Figure 12: Comparision of test and analysis torque vs. thrust for two RPMs.

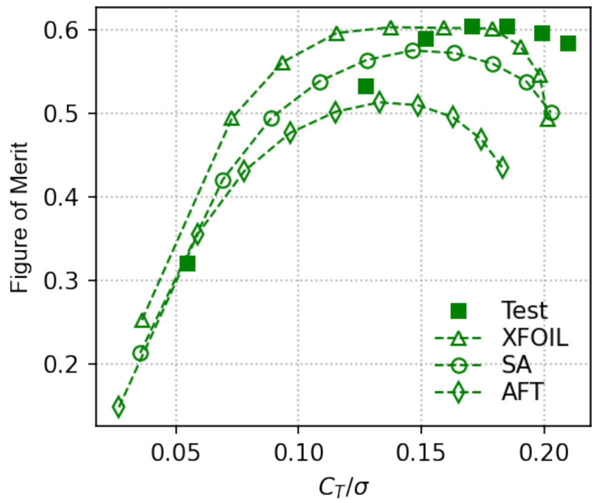

(a) 4000 rpm

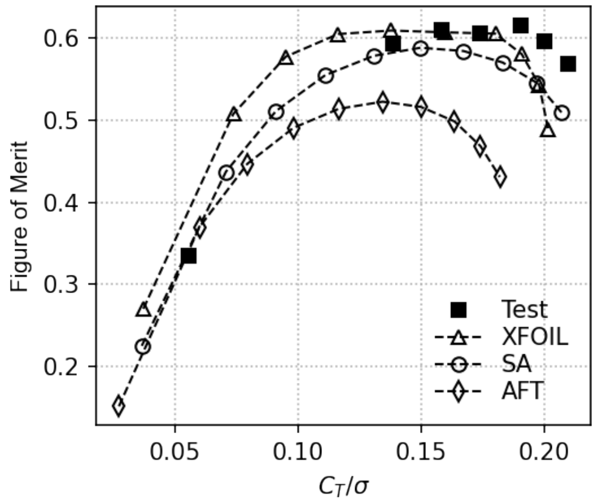

(b) 5000 rpm

Figure 13: Comparision of test and analysis figure of merit with varying collective for two RPMs.

5.2 Forward Flight

Comprehensive analysis of an isolated propeller in forward flight at three fixed collective (θ_{75}) values of 25°, 30° and 35° was performed, sweeping propeller operating speed from 1,500 to 6,000 rpm at 50 and 70 kt, SL/ISA conditions. This represents a portion of the planned operating conditions for the upcoming SCARTA wind tunnel test entry and is within the range of interest for propeller performance for typical SUAS aircraft. The CAMRAD II general free wake geometry was used, with the standard hover wake settings and the initial wake convection model applied to the first 0.3 revs of wake. As with the static thrust, a collective offset of -2° for XFOIL and -3° for SA tables is assumed.

Figure 14 shows comparison of results between XFOIL and SA airfoil tables at 50 kt with varying RPM. The two airfoil table results generally agree in terms of trends and values, though the SA shows stronger evidence of stall at the highest collective setting and highest RPM (lowest advance ratio μ_z). Both methods appear to agree on the optimal advance ratio for peak propulsive efficiency, although the XFOIL tables predict slightly higher peak efficiency, similar to the results seen for figure of merit in the static thrust case. Similar results are seen in Figure 15 for the 70 kt case. The most noticeable difference between the two different airfoil tables is related to the rate of loss of thrust with advance ratio at fixed collective. The SA model approaches zero thrust at a slightly higher advance ratio, and this contributes to the slower loss of propulsive efficiency at advance ratios above the value that corresponds to peak efficiency. Further validation of these results with single propeller wind tunnel data gathered using SCARTA is planned for Fall 2023.

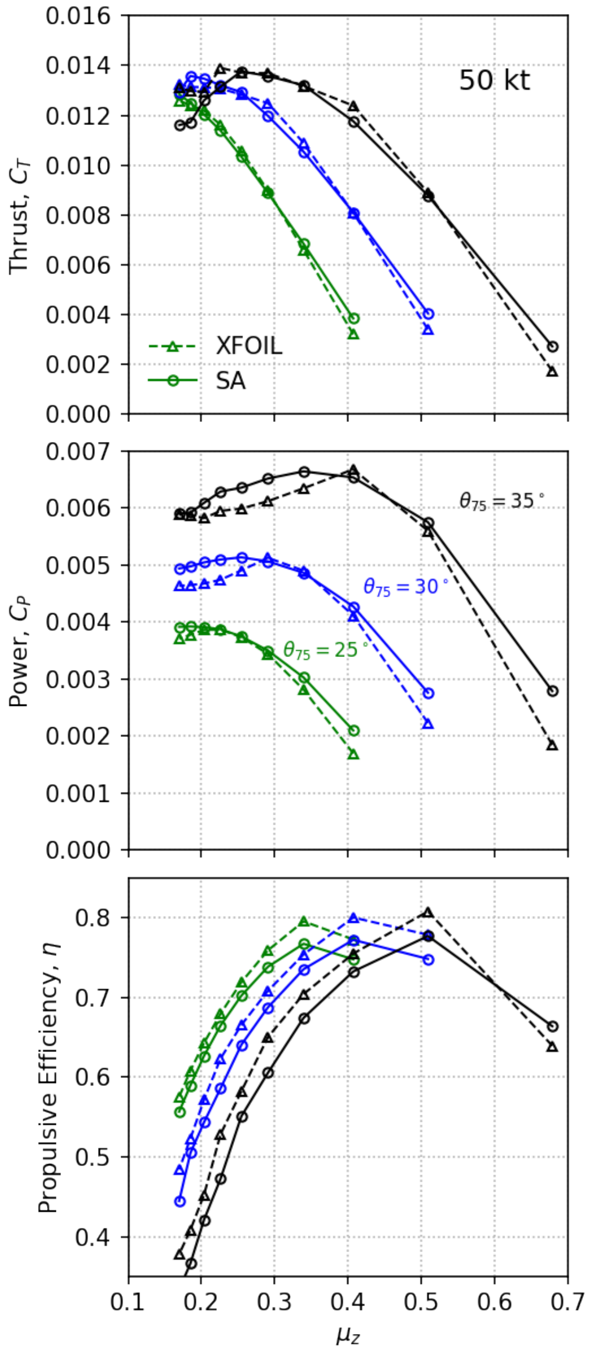

Figure 14: Propeller performance comparison between XFOIL and SA for 50 kt and various collective settings

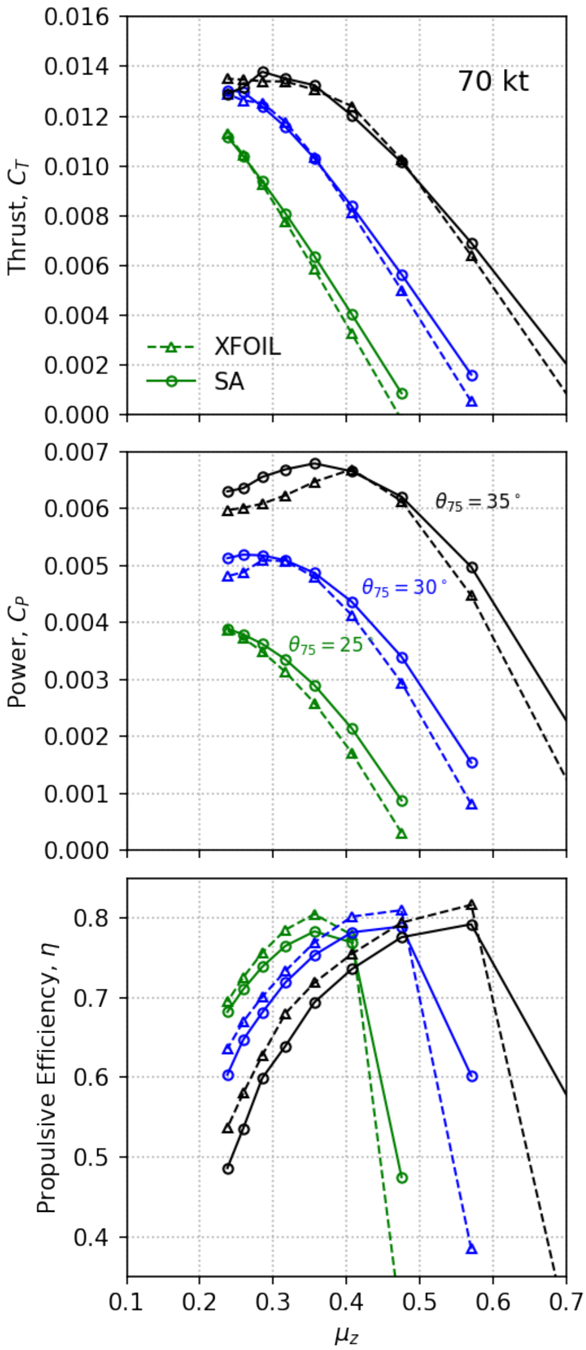

Figure 15: Propeller performance comparison between XFOIL and SA for 70 kt and various collective settings

6. COAXIAL PROPELLER ANALYSIS

Based on the results of the single propeller analysis, further exploration of coaxial propellers is conducted using CA with the SA airfoil tables. CAMRAD II's general free wake geometry model is used to ensure calculation of the mutual interference between the two propeller wakes in axial flight. As with the single propeller, the settings for hover free wake are used, but this time based on the coaxial rotor wake calibration (Ref. 13). This coaxial wake model has previously been validated against traditional coaxial helicopter rotors. Limited information is available for coaxial propellers in axial forward flight and future testing with SCARTA will hopefully provide the desired validation data. Ideal test results would include both performance and wake geometry information to help with code validation.

Figure 16 shows the variation in thrust, power and efficiency for the coaxial propeller setup at 50 kt. Here the collective pitch for the upper and lower propellers is set to the same value, and the two propeller collectives are not trimmed to balance torque. At low RPM, high advance ratio, the two propellers are essentially torque balanced at the same collective setting. As RPM is increased, advance ratio decreases and the difference in thrust and power between the two propellers increases. The aft propeller, which operates in the wake of the forward propeller, shows high power required due to unfavorable interference from the forward propeller wake. The impact of interference on thrust, is more complicated. For the highest collective setting, at low advance ratio the wake from the forward propeller helps to delay stall on the aft propeller. This is seen in Figure 16 by the aft propeller's ability to achieve higher C_T than was seen under similar operating conditions in Figure 14. At lower collective settings, where stall was not apparent in the single propeller cases, this phenomenon of the aft propeller carrying more thrust than the front propeller is not evident.

In addition to the fixed collective case, a second case was run where the collective on the aft propeller was adjusted so that torque balance is achieved between the propellers. Rotational speed between the two propellers is held constant, which is an important constraint for the analysis because of limitations in CAMRAD II's general free wake model which only allow for fully interacting wakes if the RPM of the propellers is the same. RPM variation would limit the propeller interaction to mean inflow variations only, or require significantly more computational expensive fully transient analysis in CAMRAD II. Figure 17 shows the variation in collective and thrust for the aft propeller. At lower advance ratios, aft propeller collective needs to generally be lower to achieve torque balance, but the difference required diminishes as advance ratio increases. The variation in thrust between the two propellers is also largest at low advance ratios, while being insignificant at high advance ratios. The sign of the thrust variation changes as front propeller collective is increased.

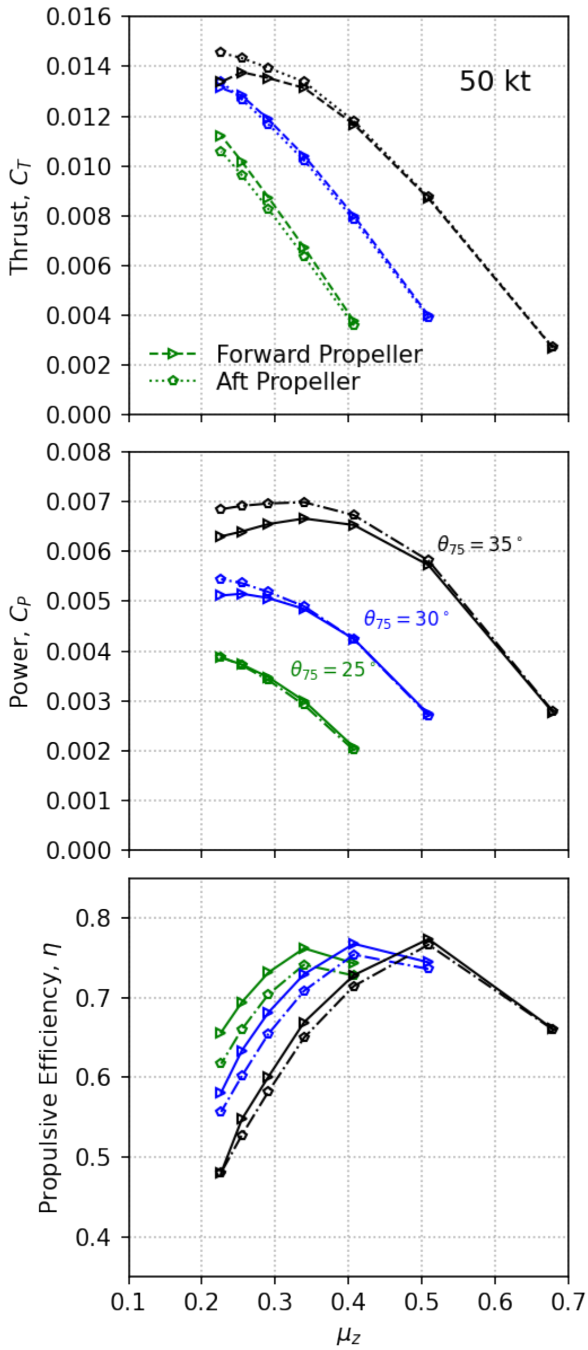

Figure 16: Predicted coaxial propeller performance variation with advance ratio at 50 kt and 3 collective values using SA airfoil tables.

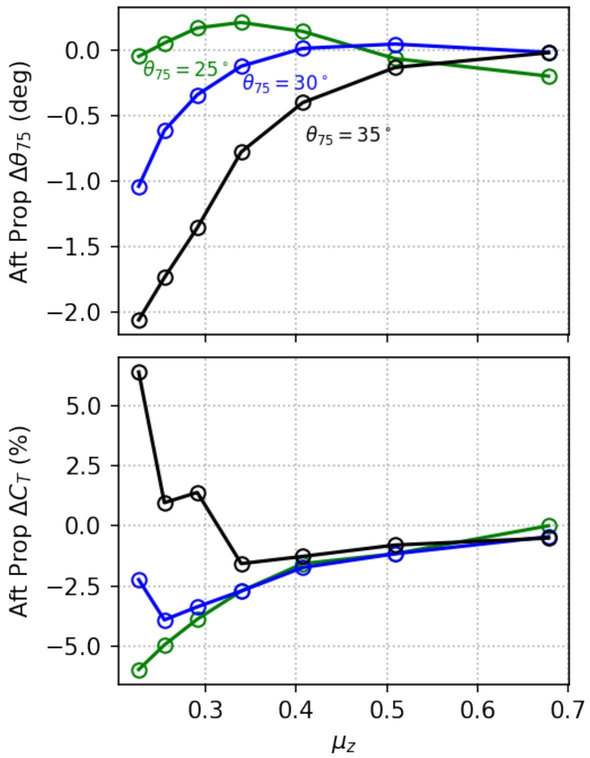

Figure 17: Predicted variation in collective and thrust for aft propeller when trimmed for torque balance.

7. CONCLUSIONS

Two dimensional airfoil properties were generated using multiple methods for SUAS class propellers. This data was used in CA to compare with static thrust and power measurements to validate the modeling approach. SUAS propellers of this size operate in a challenging Reynolds number range for airfoil section property predictions. None of the airfoil property generation methods examined gave completely satisfactory results when compared with the complete propeller performance. Airfoil data generated using the more recent laminar-turbulent boundary layer transition models, such as AFT, generally provided the least accurate correlation. Further work is needed to validate these models by correlating with experimental data of representative airfoil shapes at Reynolds numbers representative of SUAS operating conditions. Challenges continue to exist with regards to accurate prediction of $C_{\ell,\max}$ and drag variation with lift. Experimental measurement of wake geometry for this scale propeller would also help validate several inputs needed to initialize the CA free wake model.

Differences in predictions between CA using different airfoil tables appeared to be less pronounced in forward flight. Trends seen were similar with those seen previously in other studies of SUAS propellers. For coaxial propellers variation in thrust and power between the two propellers was seen to be more pronounced at lower advance ratios. A single differential setting of collective between the two propellers will not result in torque balance across the full range of operating conditions. Variation in RPM between the two propellers is likely needed to achieve trimmed torque. Future work will include validation of these results with wind tunnel test results. This validation can be aided by gathering not only force and moment information, but also wake geometry. Experiments should also examine blade deflection to confirm that elastic effects are small.

8. ACKNOWLEDGMENT

The authors wish to thank the Army Ames 7x10 Wind Tunnel Support Staff for their help in assembly, setup and debugging of the SCARTA test rig. Ananth Sridharan's help in setting up AFTGen to run on Narwhal, enabled the rapid turn around of large airfoil data sets, thereby making it practical to explore airfoil variations in the analysis.

9. REFERENCES

1. Battey, L. and Russell, C., "Wind Tunnel Testing a Small Isolated Folding Propeller," 76th Annual Forum of the Vertical Flight Society, October 2020.

2. Kang, H., Anusonti-Inthra, P., Singh, R., and Battey, L., "Performance Predictions of a Small Propeller Using Rotorcraft Comprehensive Analysis," VFS Aeromechanics for Advanced Vertical Flight Technical Meeting, January 2022.

3. Cornelius, J. and Schmitz, S., "Rotor Performance Predictions for UAM Single vs Coaxial Rigid Rotors," VFS's Aeromechanics for Advanced Vertical Flight Technical Meeting, January 2022.

4. Russell, C. R. and Sekula, M. K., "Comprehensive Analysis Modeling of Small-Scale UAS Rotors," AHS International 73rd Annual Forum Proceedings, May 2017.

5. Maughmer, M. D. and Coder, J. G., "Comparisions of Theoretical Methods for Predicting Airfoil Aerodynamic Characteristics," Technical Report RDECOM TR 10-D-106, U.S. Army Research, Development and Engineering Command, Port Matilda, PA, August 2010.

6. Coder, J. G., “Further Development of the Amplification Factor Transport Transition Model for Aerodynamic Flows,” Paper AIAA-2019-0039, AIAA SciTech, January 2019.

7. Kallstrom, K., “Exploring Airfoil Table Generation Using XFOIL and OVERFLOW,” VFS's Aeromechanics for Advanced Vertical Flight Technical Meeting, January 2022.

8. Davis, J. M., “Rotorcraft Flight Simulation with Aeroelastic Rotor and Improved Aerodynamic Representations, Volume II – Users's Manual,” Technical Report USAAMRDL-TR-74-10A, Bell Helicopter Company, Fort Eustis, VA, June 1974.

9. Drela, M., *XFOIL: An Analysis and Design System for Low Reynolds Number Airfoils*, Lecture Notes in Engineering, Springer Berlin Heidelberg, 1989. doi: 10.1007/978-3-642-84010-4

10. Derlaga, J. M., Jackson, C. W., and Buning, P. G., “Recent Progress in OVERFLOW Convergence Improvements,” Proceedings of AIAA SciTech Forum, January 2020.

11. Johnson, W., “Technology Drivers in the Development of CAMRAD II,” American Helicopter Society Aeromechanics Specialist Meeting, January 1994.

12. Du, Z. and Selig, M. S., “A 3-D Stall-Delay Model for Horizontal Axis Wind Turbine Performance Predictions,” AIAA Aerospace Sciences Meeting, January 1998.

13. Lim, J. W., McAlister, K. W., and Johnon, W., “Hover Performance Correlation for Full-Scale and Model-Scale Coaxial Rotors,” *Journal of the American Helicopter Society*, Vol. 54, (3), 2009.